



The 3D Probabilistic Analysis of the Effect of Pre-support Systems on the Surface Settlement in Conditions of Spatial Variability of Soil Properties: A Case Study

Mohammad Ali Tahmasebi¹ · Reza Shirinabadi¹ · Esmail Rahimi¹ · Ehsan Moosavi¹ · Amir Hossein Bangian Tabrizi¹

Received: 8 January 2021 / Accepted: 17 March 2022 / Published online: 6 April 2022
© Saudi Society for Geosciences 2022

Abstract

In order to prevent the excessive surface settlement in urban tunnels, especially when the tunnel overburden is low, either a sequential excavation method (SEM) or soil reinforcement techniques, or a compound of both, can be employed. To improve operations of excavation and reduce surface settlement in Zarbalizadeh tunnel, new Austrian tunneling method (NATM) and two pre-support systems were designed and implemented. To investigate the effect of pre-support systems on maximum surface settlement (S_{\max}), the soil behavior must be carefully evaluated. In this regard, random finite difference method (RFDM) has been used to describe the real soil conditions and four probable scenarios were considered based on the presence or absence of pre-support systems. Then, the S_{\max} values for different scenarios were obtained and compared to one another. The results of this research reveal that in case of a lack of pre-support systems, both the percentage changes of the mean of S_{\max} and its coefficient of variation (COV) were increased by 84.2% and 61.0%, respectively.

Keywords Spatial variability · Scale of fluctuation · NATM tunnel · Surface settlement · Pre-support system

Introduction

Excessive surface settlement is one of the major problems we encounter when constructing shallow tunnels in soft grounds. In such situations, pre-support systems are implemented to stability of the excavation face and reduce tunnel deformation (Moosavi et al. 2018). So far, in order to study the influence of pre-support systems, the subject of spatial variability of soil properties has not been considered. Ignoring this issue leads to an underestimation of the risk of excessive surface settlement (Xiao et al. 2017), and as a result, we cannot have an accurate interpretation of the impact of the pre-support system. In this regard, it is necessary to accurately determine the soil properties. Under natural conditions, due to sedimentary and sedimentation processes, the soil is layered inhomogeneously and anisotropically (Cheng et al. 2019b; Dasaka and Zhang 2012).

Therefore, soil parameters in different places show different values, which is interpreted as spatial variability of soil (Fenton and Griffiths 2005). In this case, soil properties show high heterogeneity at different spatial scales, which causes uncertainty in estimating soil parameters and poses a critical challenge in describing soil over large areas. Thus, to achieve the real condition of the soil, the spatial variability of the soil must be simulated in numerical modeling. Conventional methods do not have the ability to simulate and describe random spatial variability of soil properties (Marinos et al. 2019). Therefore, the use of new methods seems necessary. One of these methods is the theory of random fields (RF). A normalized random field is a random process where the parameters are not limited to only simple real-time or integer values, but they can also be multidimensional vectors.

A random field, in its simplest form, is a list of random numbers each referring to a point in space. Random data are often interconnected in space through one or more paths. Such data can be defined in a continuous domain and can form a random space like a random data function. Based on the theory of RF, it is possible to study the effect of the spatial variability of soil parameters for urban tunnels. One of the most complex methods of generating a RF is RFEM

Responsible Editor: Murat Karakus

✉ Reza Shirinabadi
r_shirinabadi@azad.ac.ir

¹ Department of Mining and Petroleum Engineering, South Tehran Branch, Islamic Azad University, Tehran, Iran

(Griffiths and Fenton 2008). RFEM is a compound of RF theory, the finite element method and the Monte-Carlo simulation (MCS). RFEM requires considerable computational power, especially if this type of analysis is performed in three dimensions (3D) for a considerable number of MCS. This can be one of the reasons for the limited number of articles that study the three-dimensional effects of spatial of variability soil properties in NATM tunneling operations.

Recently, a number of researchers have studied the effect of soil variability on surface settlement caused by the tunnel construction. Molon et al. (Mollon et al. 2013) propounded a two-dimensional random numerical method based on MCS to study the Influence of soil friction angle variation. Cheng et al. (Cheng et al. 2019b) studied the stability of the two-dimensional excavation face in various soils and then investigated the effect of soil shear strength on the reliability and failure mechanism of the tunnel face. Miro et al. (Miro et al. 2015) studied the types of distribution of soil parameters on surface settlement and suggested a method to decrease the uncertainties of soil parameters. The property of soil variability is extensively acknowledged by researchers, and its effect on the underground structures has been considered in the literature (Cheng et al. 2019a, 2019b, 2019c; Vanmarcke 2010). Given the fact that among soil parameters the Young's modulus (E) has the greatest effect on soil deformation (Fenton and Griffiths 2002; Griffiths and Fenton 2004; Li et al. 2015; Phoon and Kulhawy 1999), the spatial variability of E is modeled using a three-dimensional RF. Also, the scale of fluctuation (SOF) is used to measure the correlation of Young's modulus parameter. RFs of soil's Young's modulus are generated by the Fourier series method (FSM) and mapped onto the finite difference mesh. Sensitivity studies are further carried out via MCS.

The structure of this study is as follows. First, the parameters required to create a RF are examined, and then the necessary functions to create a three-dimensional RF is presented; second, a numerical model is created based on the geological conditions and excavation method for Zarbalizadeh project and the numerical model is verified with field data from tunnel instrumentations; third, the 3D RFs are generated for the Young's modulus and assigned to the 3D finite difference mesh. Finally, a parametric analysis is performed based on MCS to study the effects of pre-support systems on S_{\max} .

Basic concepts of RF

Determination of SOF

Under natural conditions, the soil is layered horizontally. Intrinsic spatial variability of soil properties resulting

from sedimentation processes is one of the main problems of the stability of tunnel face in urban shallow soft grounds (Zhou et al. 2019). To accurately describe soil behavior, the theory of RFs can be a desirable way to investigate the spatial structure of soil parameters. In RF theory, the SOF is propounded to quantify the spatial extent. In other words, an appropriate way to measure the rate of variability of RF is the SOF (Vanmarcke 1983). That is, if the interval between 2 points is less than SOF, the properties of soil at these points are strongly associated and vice versa. If the interval is greater than the SOF, a weak association occurs. In other words, a large value of the SOF indicates that the properties of the soil on a large scale are extremely correlated. Thus, a smooth RF is created (Jaksa et al. 1997). When the limit of the SOF tends to infinity, the homogenous and various RF is generated for each realization (because of the effects of the coefficient of variation (COV) (Bagińska et al. 2016)). On the other hand, Cherubini (Cherubini 1997) states that the values of the vertical SOF is usually smaller than the horizontal one and soils commonly expose an intense correlation in the horizontal direction. So far, methods for determining vertical SOF ("depth variability") have been defined, but they have not been favorably developed for horizontal SOF. Since no data about the horizontal SOF of the Zarbalizadeh tunnel project soil is available in the prior literature, a parametric study is performed for different horizontal SOF values. Both horizontal SOFs (namely Θ_x and Θ_y) are assumed to be equal. Due to the time-consuming calculations in 3D, only a constant value of the vertical SOF is chosen as a value of representative for computations. In order to study RF, it is required to define a statistical distribution corresponding to the project geological conditions. Among the cumulative distribution functions, the log-normal distribution is consistent with the statistical specification and deposition processes of soil. Accordingly, the log-normal distribution is considered herein to describe the variability of the Young's modulus (Huang et al. 2013).

Generation of RFs

The application of stochastic field theory to geotechnical problems was first reported in the 1960s (Lumb 1966). In recent decades, with the advancement of technology and the increasing computing power of computers, the use of stochastic field theory in considering spatial variables has become particularly important. There are different types of the correlation function of soil parameters. One of the common correlation functions used to generate RF is the Markov-type function, which is defined as follows:

$$\rho(\tau_x, \tau_y, \tau_z) = \exp\left(\frac{-2|\tau_x|}{\theta_x} + \frac{-2|\tau_y|}{\theta_y} + \frac{-2|\tau_z|}{\theta_z}\right) \tag{1}$$

where the correlation function $\rho(\tau_x, \tau_y, \tau_z)$ = a function of the horizontal distances τ_x, τ_y and the vertical distance τ_z between any two points in the spatial extent. Parameters θ_x, θ_y and θ_z are SOF in the directions x, y and z, respectively. Since the correlation between data is logarithmic in the log-normal distribution, real-scale correlation cannot be guaranteed. Therefore, by the suitable transformation of normal RF, a log-normal RF should be converted to RF that model soil properties (Fenton and Griffiths 2003). If the Young’s modulus is considered to be a log-normal RF ($Y(x), x \in D$ and D is a 3D domain), the converted field is created from a normal RF($X(x)$) by using the following function (Fenton and Griffiths 2003; Griffiths and Fenton 2001)

$$Y(x) = \exp(X(x)) \tag{2}$$

The probability density function of $Y(x)$ for a given point such as x is determined by Eq. (3) which is defined as:

$$f(t) = \begin{cases} \frac{1}{t\sigma_{\ln Y}\sqrt{2\pi}} \exp\left\{-\frac{1}{2}\left(\frac{\ln t - \mu_{\ln Y}}{\sigma_{\ln Y}}\right)^2\right\}, & t > 0 \\ 0, & t \leq 0 \end{cases} \tag{3}$$

where $\sigma_{\ln Y}$ and $\mu_{\ln Y}$ are the standard deviation and the mean value of $X(x)$, respectively. The standard deviation σ_Y and mean value μ_Y of the $Y(x)$ ($Y(x)$ is log-normal distribution) are related to $\sigma_{\ln Y}$ and $\mu_{\ln Y}$ by:

$$E[Y] = \mu_Y = \exp\left(\mu_{\ln Y} + \frac{1}{2}\sigma_{\ln Y}^2\right) \tag{4}$$

$$\sigma_Y^2 = \mu_Y^2(\exp(\sigma_{\ln Y}^2) - 1) \tag{5}$$

To consider the range of Young’s modulus, Fenton and Griffiths (Fenton and Griffiths 2003, 2008) presented the following transformation:

$$Y(X) = a + \frac{1}{2}(b - a) \left[1 + \tanh\left(\frac{m + sX_0(x)}{2\pi}\right) \right] \tag{6}$$

where $X_0(x)$ is the standard normal random variable, and distribution’s parameters are s and m . The function of $Y(x)$ is also defined at the interval $[a,b]$ (a and b are the smallest and the greatest values of the Young’s modulus variation range, respectively). Finally, the probability density function of $Y(x)$ takes the form:

$$f(t) = \begin{cases} \frac{\sqrt{\pi}(b-a)}{\sqrt{2s(t-a)(b-t)}} \exp\left\{-\frac{1}{2s^2}\left[\pi \ln\left(\frac{t-a}{b-t}\right) - m\right]^2\right\}, & t \in (a, b) \\ 0, & t \notin (a, b) \end{cases} \tag{7}$$

The following approximation is obtained through the use of the third-order Taylor’s expansion:

$$\sigma_Y^2 \approx \frac{1}{4}(a - b)^2 \frac{s^2}{4\pi^2 + s^2} \tag{8}$$

Project Overview

The Zarbalizadeh underpass project in Tehran has been considered to pass through the corridor subway-railway and join the Zarbalizadeh street to Maddah street. Moreover, this underpass is located between the south terminal subway station and Khazaneh subway station. The purpose of executing this project in district 16 of Tehran is to connect the eastern–western parts between two urban areas. The tunnel is 44 m long, and the overburden cover on the tunnel is 3.5 m. The height between the invert and the tunnel crown is 11.55 m, and the width is 14.14 m. In addition, this tunnel was excavated with the NATM method. The analysis and the design of this project were based on reliable references such as: FHWA-NHI-10-034, FHWA-NJ-2005-002, AASHTO, ACI 318-05 and the international tunneling and underground space association (ITA) guidelines for the design of tunnels. It should be noted that the project was recognized in 2018 by ITA in China as the world’s leading tunnel projects (in the section of tunnel projects with a credit of less than 50 million euros). Figure 1 shows the situation of the project site, and Fig. 2 illustrates the cross-section and longitudinal profile of Zarbalizadeh tunnel.

The geological engineering conditions

According to the in situ and laboratory tests, the geotechnical characteristics of different layers of the project are shown in Table 1 (Karamniayi and Dehghan 2019). The longitudinal geological profile of tunnel route is shown in Fig. 3. According to Fig. 3, the tunnel route is located within the “D2-1” geological layer. Thus, the soil properties in this area are used for the numerical analysis. According to studies, the underground water is relatively deep, and the Zarbalizadeh underpass is located above it.

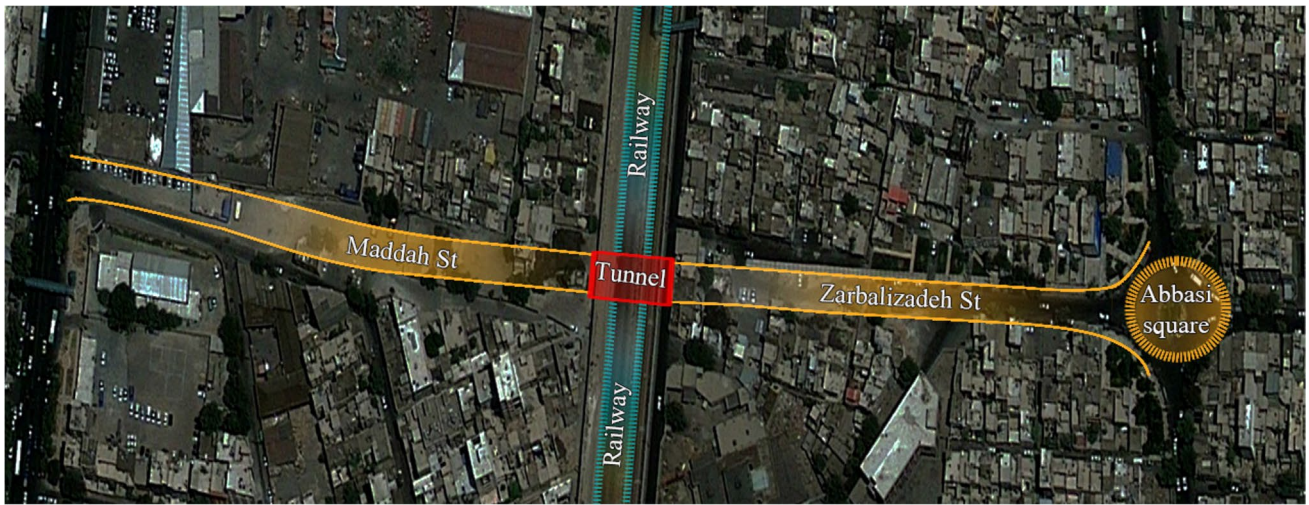


Fig. 1 The plan of Zarbalizadeh tunnel project in urban area in Tehran, Iran

Fig. 2 a Longitudinal slope profile along the route of the tunnel, ramps and cut-and-cover zones and (b) geometric properties of the tunnel section

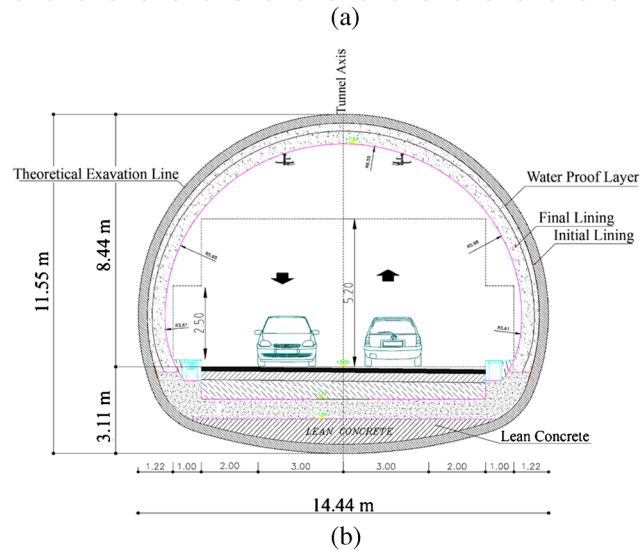
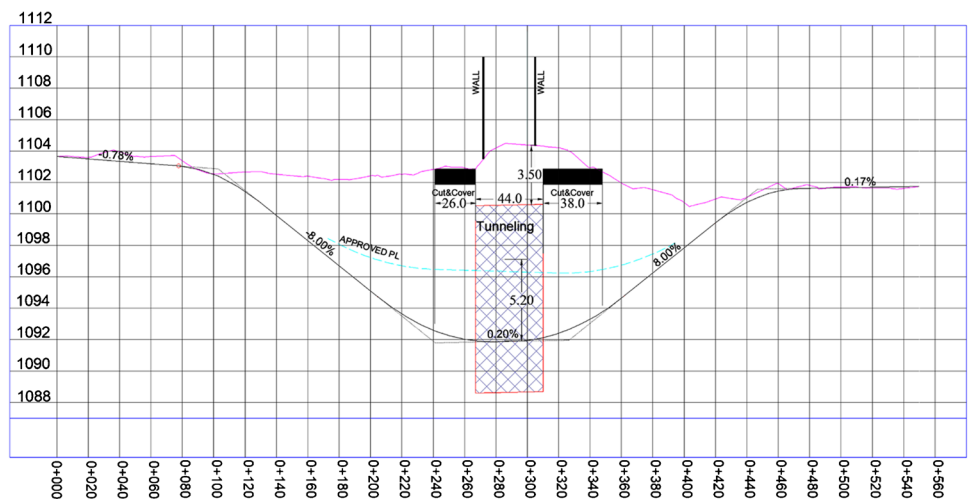


Table 1 Geotechnical properties of soil layers

Type	Cohesion C (kg/cm ²)		Friction angle Φ (deg)		Elastic modulus E (kg/cm ²)	Poisson's Ratio	Unit weight γ (g/cm ³)			Consolidation (kg/cm ²)		
	C'	C _{cu}	φ	cuφ			Dry	Wet	Sat	Cc	Cs	Pc
D2-2	.32 ± .1	.42 ± .1	27 ± 2	20 ± 2	260 ± 50	0.30	1.65 ± 0.1	1.80 ± 0.1	1.85 ± 0.1	.2-.3	0.03–0.04	3–3.5
D2-1	.30 ± .1	.36 ± .1	28 ± 2	21 ± 2	280 ± 50	0.30	1.60 ± 0.1	1.80 ± 0.1	1.85 ± 0.1	.1-.2	0.03–0.04	2–2.5
D1-2	.31 ± .1	.30 ± .1	30 ± 2	23 ± 2	300 ± 50	0.32	1.65 ± 0.1	1.80 ± 0.1	1.85 ± 0.1	.2-.3	.02-.03	2.8–3.2
C1	.20 ± .1	.25 ± .1	34 ± 2	25 ± 2	520 ± 50	0.31	1.70 ± 0.1	1.85 ± 0.1	1.90 ± 0.1	.15-.25	.025-.035	2.5–3.5
B	.12 ± .1	.20 ± .1	35 ± 2	30 ± 2	600 ± 50	0.31	1.80 ± 0.1	1.90 ± 0.1	1.95 ± 0.1	-	-	-

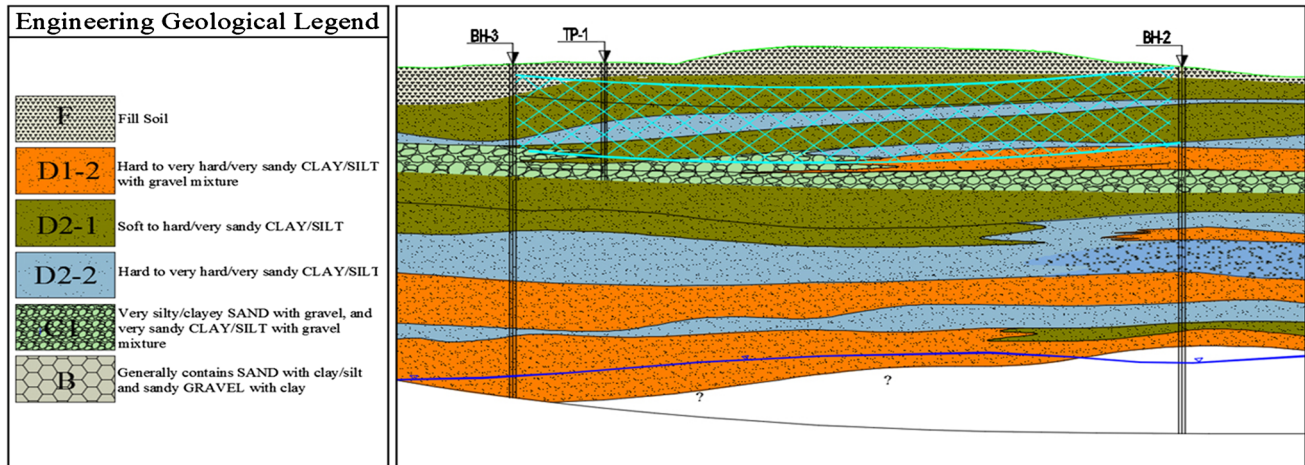


Fig. 3 Longitudinal geological profile of tunnel route

Excavation method

In urban spaces, ground movement induced by the tunnel excavation may cause serious damage to nearby structures. One of the popular methods for tunnel design and construction in urban areas is NATM (Taromi et al. 2017). Due to the flexibility in adapting to different geological conditions and the use of simple equipment, this method is used for excavating urban tunnels in many countries. Displacements induced by NATM tunneling can be controlled by adjusting the excavating speed, the reduction of distance between the tunnel face and the support systems, the selection of the partial-face excavation instead of the full-face excavation and the reduction of time to invert closure (He et al. 2019). One of most common patterns in NATM is the side drifts method (SDM) which is widely used in the soft grounds through decreasing the excavating cross-section area. Considering the low overburden length and the large span of the Zarbalizadeh tunnel, the full-face excavation was not possible, and therefore, the SDM was selected for this project.

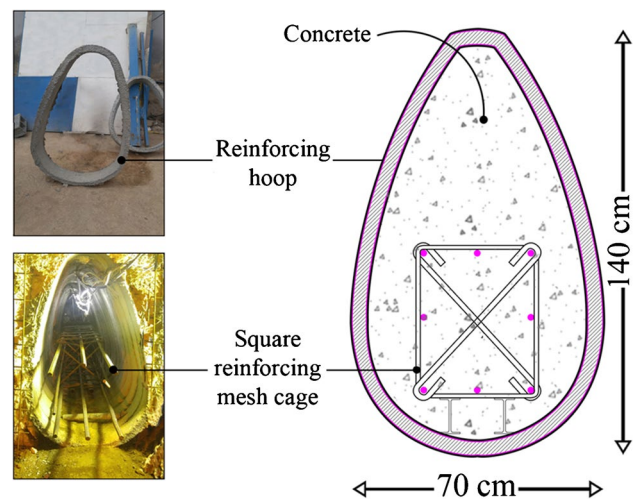


Fig. 4 Geometry of progressive beam consisting of the reinforcing hoop and square reinforcing mesh cage

Support systems

The support systems utilized in Zarbalizadeh tunnel comprise the pre-support and the main support systems.

Pre-support systems

A. Progressive beam (a type of Innovative soil pre-support system): It can be called a micro tunnel with a very small cross-section (about 0.7m^2) which is excavated full-face and lined with reinforcing hoops. Then inside each micro-tunnels, the square reinforcing mesh cages are placed and filled with concrete (Fig. 4). In this project, 5 progressive beams with a length of 44 m (equal to length of tunnel route) were considered. Their locations are shown in Fig. 8.

B. Forepoling umbrella system (FUS): It is consisted of 36 steel pipe elements (forepoles) with an outside diameter of 76 mm, a length of 8 m, an installation angle of 8° and a center-to-center spacing of 50 cm. Forepoles are installed every 2 m to create a 6 m overlap between successive forepole umbrellas (Fig. 5). The forepoles installation locations are shown in Fig. 8.

Main support system

A. Composite support system: it is an initial support system which is installed immediately after the excavation to prevent excessive ground deformation and increase tunnel stability (Fig. 7a).

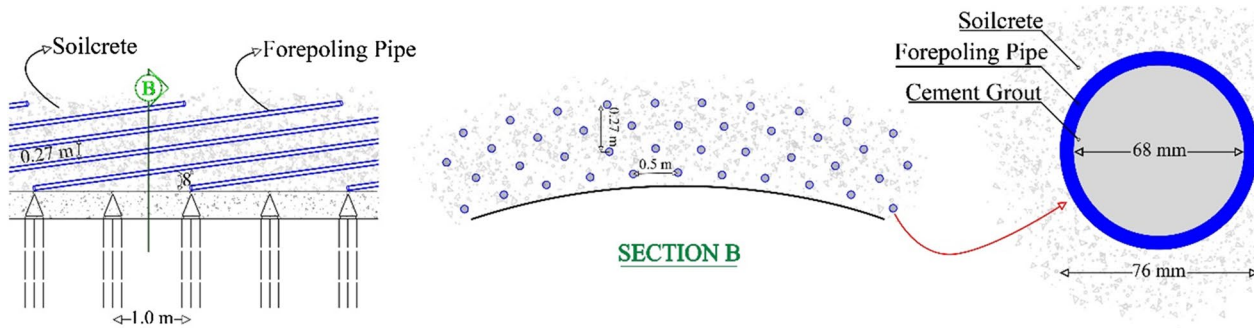


Fig. 5 Schematic illustration of forepoling umbrella system components in the longitudinal and transversal cross-section

Fig. 6 Geometry of composite support system: (a) permanent and (b) temporary support (Not to scale)

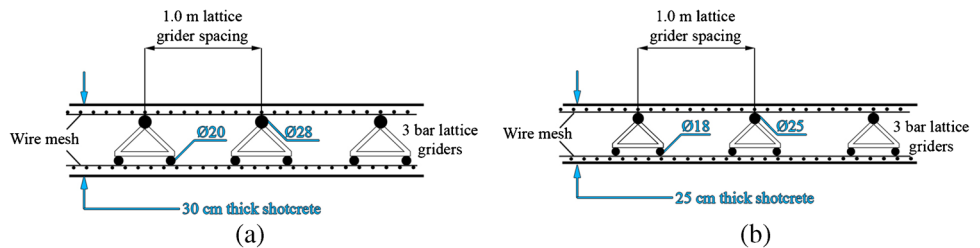


Fig. 7 Main support systems in studied case: (a) composite support system (b) final lining



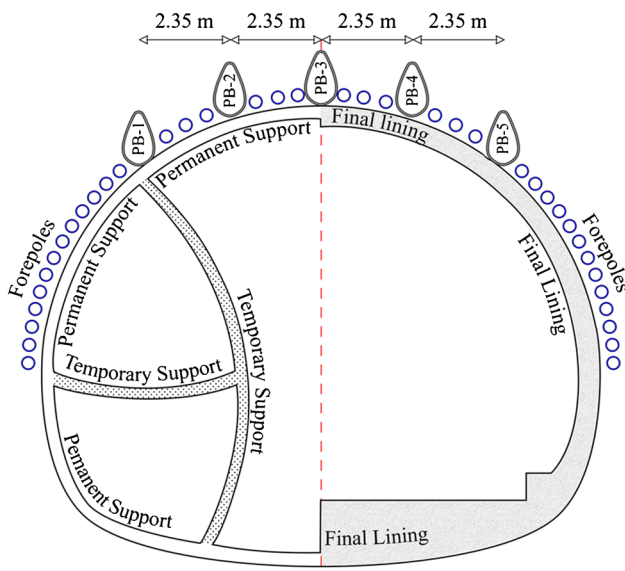


Fig. 8 View of all support systems consisting of lattice girders embedded in shotcrete (composite support system), progressive beams (PB), forepoling umbrella system (FUS) and concrete final lining

- 1) Permanent support: It is consisted of a welded wire mesh and 3 bar lattice girders (steel type AIII ($\varnothing = 20, 28$) which is embedded in a 30 cm thick shotcrete lining (Fig. 6a).
- 2) Temporary support: It is consisted of a welded wire mesh and 3 bar lattice girders (steel type AIII ($\varnothing = 18, 25$) which is embedded in a 25 cm thick shotcrete lining (Fig. 6b).

The composite support system is installed at the interval of 1m from the excavation face.

B. Lining: it is a final support system (Fig. 7b). The physical parameters of the lining structure and the design used in the analysis and design are as follows:

Concrete with the Compressive failure strength equal to $f_c = 300 \text{ kg/cm}^2$, the elastic module equal to $E_c = 26 \times 10^4 \text{ kg/cm}^2$ and unit weight equal to $\rho_c = 2500 \text{ kg/cm}^3$.

Reinforcing steel (steel type AIII) with compressive strength equal to $f_y = 4000 \text{ kg/cm}^2$ and elastic module equal to $E_c = 2 \times 10^6 \text{ kg/cm}^2$.

The thickness of lining segment is 50 cm.

Tunnel construction process

Before the excavation of side drifts, the excavation and the consolidation of the progressive beams are implemented along the tunnel rout for 44 m. The excavation operation is simultaneously started from both portals. Prior to the excavation operation, the forepoles are installed around the part of the drift No.1 according to Fig. 9–1 and then the excavation of this drift begins. The excavation step and unsupported span (which is defined as the distance between the excavation face and the closest installed support) are considered to be 1 m. When the drift No.1 reaches 4 m, the operation of excavation and installation of composite support system in drift No.2 (like the drift No.1) is started (Fig. 9–2). The sequential excavation is according to the drift number so that the distance between drifts (about 4 m) is kept until the excavation is completed. Therefore, when the drift No.1 and No.2 reaches 8 m and 4 m respectively (Fig. 9–3), the operations of excavation and installation of composite support systems in drift No.3 is started (when the excavation of drift No.3 is commenced, the first umbrella arc is formed). The upper drifts (No.1, 2 and 3) are completely excavated before the excavation of the lower drifts (Fig. 9–4). The excavation of the lower side drifts is continued with the destruction of the temporary wall and the temporary invert to full span. Finally, the final lining is carried out after the destruction of the temporary support (Fig. 9–5) (Fig. 8).

Numerical simulation

Geometry and Assumptions on Numerical Model

The simulation of the SDM tunneling process of Zarbalizadeh tunnel using $FLAC^{3D}$ software is started with the selection of model geometry in three dimensions. For accurate numerical modeling according to the tunnel construction process (Fig. 9), the numerical model with proper grouping is created. To ensure that there are no explicit boundary effects, the model is built with dimensions of 90 m (length) \times 44 m (width) \times 35 m (depth). Since the model is asymmetric (due to the asymmetry of the excavation sequences of tunnel drifts), the whole domain is considered in the model. The created mesh is composed of around 44,235 grid points and 85,067 zones. The bottom boundary is fixed in all directions (i.e., x, y and z) and the four vertical boundaries are fixed in the x- and y-directions, but the top boundary of the model is free and could move along the z-direction. Train load is about 93.5 Kpa (Karamniayi and Dehghan 2019) which is applied over the ground surface (the load caused by the train passing).

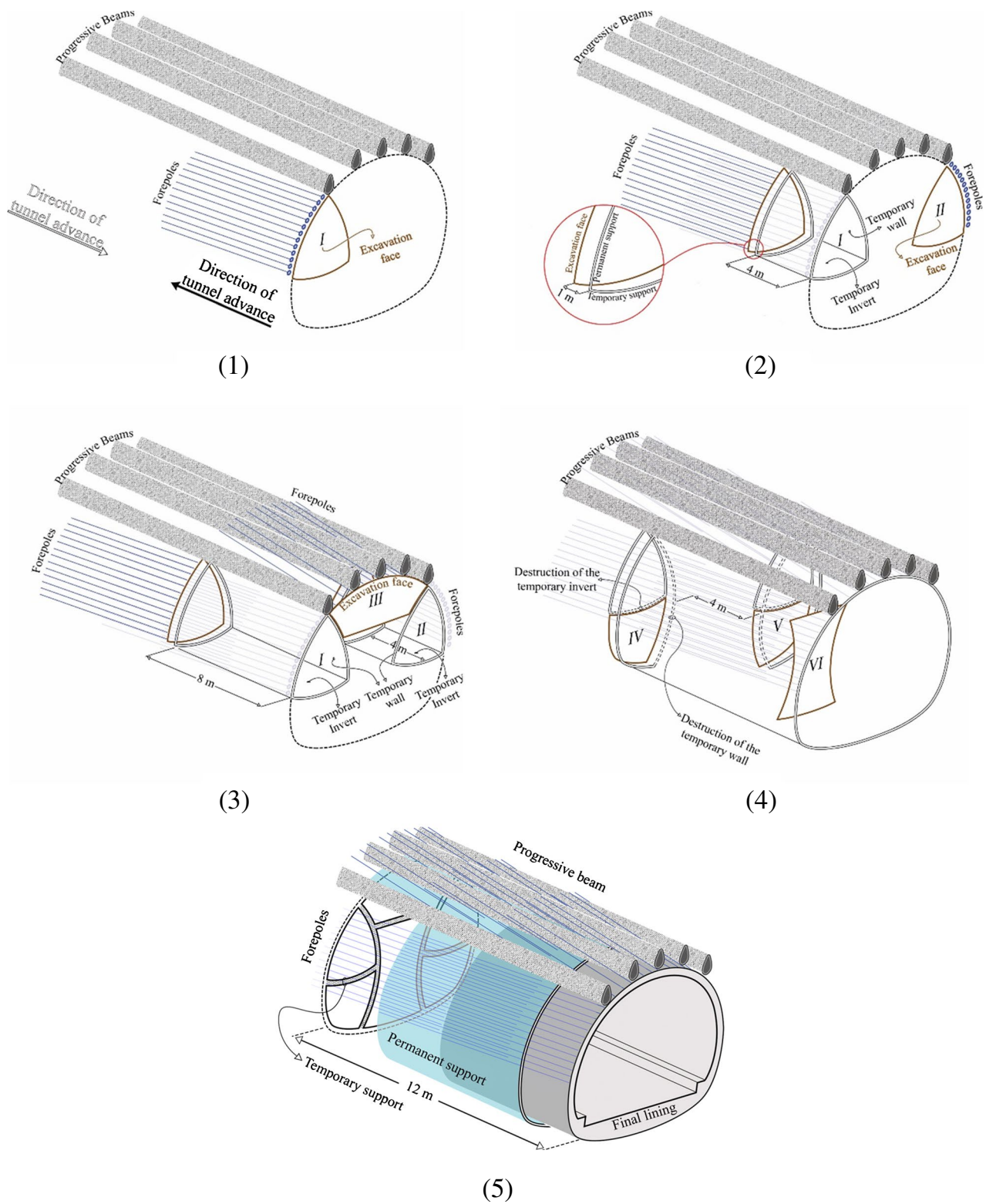


Fig. 9 Stages of tunnel construction (including sequence of excavation and installation of support system) for 12 m of the tunnel length

The soil behavior is defined by an elastic-perfectly plastic model based on the Mohr–Coulomb failure criterion. The ratio of horizontal to vertical stresses (K_0) is calculated

from the Jaky's equation ($K_0 = 1 - \sin(\varphi)$) (Jaky 1948)). The in situ stress is generated using FISH function, gravity and σ_{zz} (Fig. 10) (Table 2).

Fig. 10 Finite difference mesh, geometry of excavation stages and the numerical model boundaries

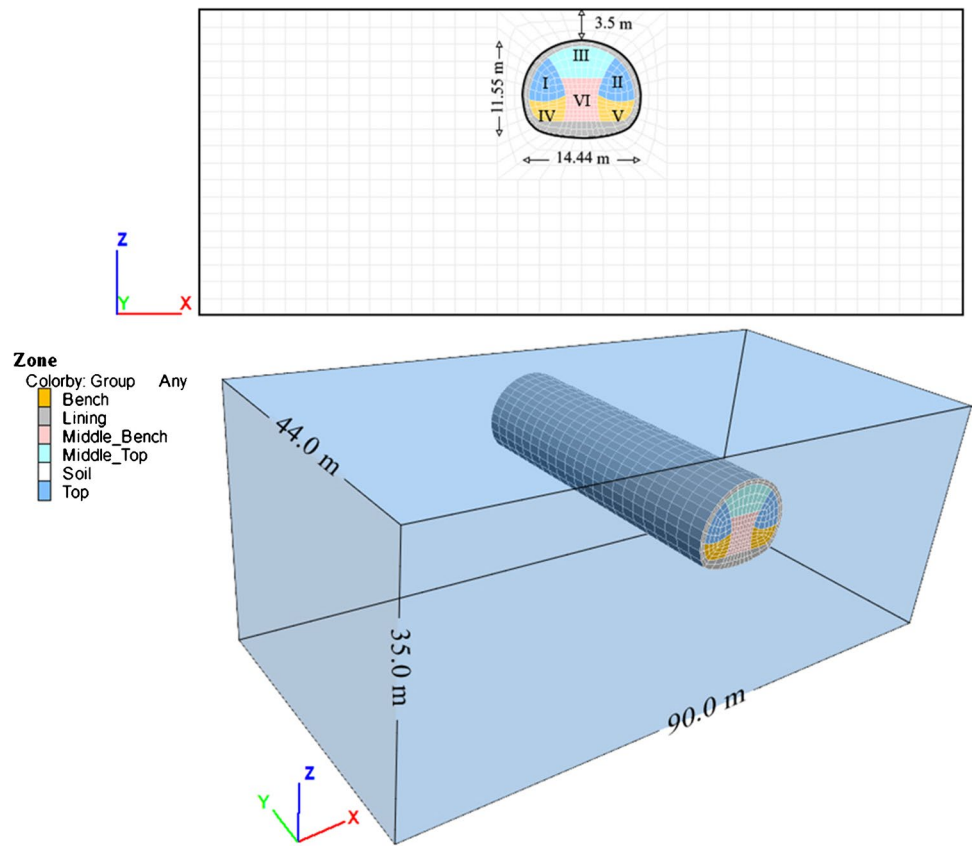


Table 2 Volumetric elements properties used in modeling

volumetric element type	Friction angel φ ($^{\circ}$)	Cohesion C (Kpa)	Unit weight (Kg/m^3)	Poisson's ratio ν	Young's modulus E(GPa)	Thickness d (cm)
Soil	28	29.5	1600	0.3	0.275	-
Soilcrete	35	4200	2300	0.25	2.6	-
Lining	-	-	2400	0.2	20	50

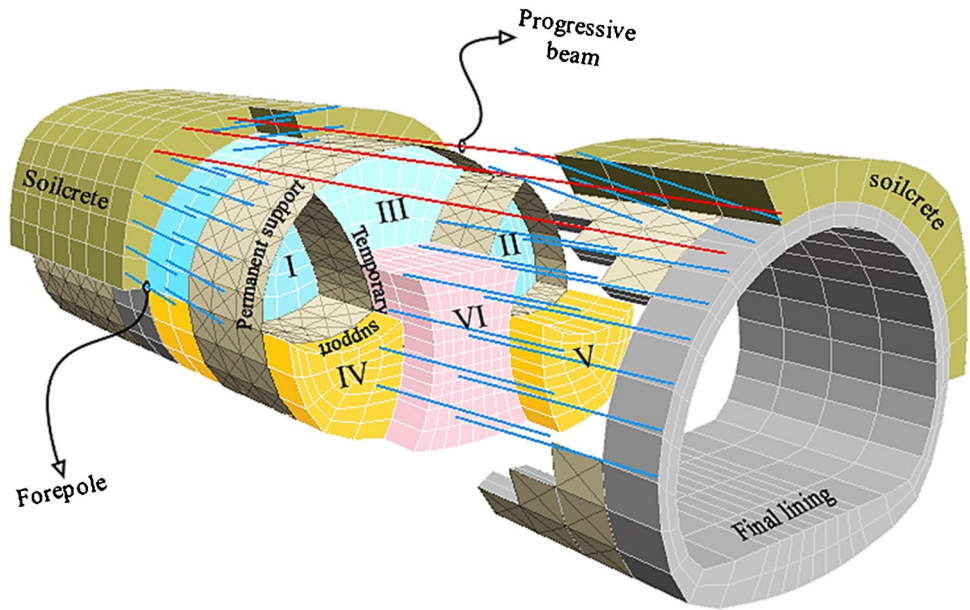
Table 3 Pre-support systems properties used in modeling

Pre-support system type	polar moment of inertia J (m^4)	Iz (m^4)	Iy (m^4)	exposed perimeter P (m)	cross-sectional area A(m^2)	Poisson's ratio ν	Young's modulus E(GPa)
Progressive beam	0.0421	0.0331	0.1052	3.532	0.854	0.3	30
Forepoling	0.00	0.0190	0.0190	0.2388	0.0045	0.3	200

Table 4 Composite support systems properties used in modeling

Composite support system type	Thickness d (cm)	Poisson's ratio ν	Young's modulus E(GPa)
Permanent support	30	0.3	15
Temporary support	25	0.25	10

Fig. 11 Stages of tunnel excavation and support systems simulated of Zarbalizadeh tunnel project in 3D modeling



Simulation of support systems

As mentioned earlier, for supporting drifts, two types of support systems were used. The progressive beam and forepoling pipes are simulated by the pile element (Table 3). Welded wire mesh, shotcrete and lattice girder are simulated by the shell element (Table 4) based on the equivalent cross-section approach introduced by Carranza-Torres and Diederichs (Carranza-Torres and Diederichs 2009). Lastly, the final lining and the improved soil around forepoling pipes (soilcrete) are modeled as volumetric elements (Fig. 10 and Table 2). The Mohr–Coulomb model was assigned to the soilcrete elements (Dehghani et al. 2020; Rahimi et al. 2020) (Fig. 11).

The complete tunnel construction process is simulated by a numerical analysis through a step-by-step approach. The unsupported span is considered in numerical modeling to accurately and realistically simulate the actual in situ conditions in the studied tunnel project. Therefore, by applying the stress reduction method, the delayed installation of the

support system and the load sharing between ground and support system are taken into account (Möller 2006).

Verification of the numerical model

Before creating RF in the finite difference mesh, the numerical model is verified based on field measurement data to ensure the accuracy of the calculations. The surface settlement is monitored by surface settlement point using leveling instruments. A monitoring Sect. (16 m away from the eastern portal of the tunnel) is considered for the verification of the numerical model into the tunnel path. The schematic view of the monitoring section in the Zarbalizadeh tunnel route is displayed in Fig. 12. As shown in the latter, point C was installed on the tunnel centerline. The ground surface settlement time curves are shown in Fig. 13.

According to Fig. 14b, the S_{max} of numerical analysis and field measuring are 28.6 mm and 30 mm respectively. Figure 14b shows the acceptable compliance between the

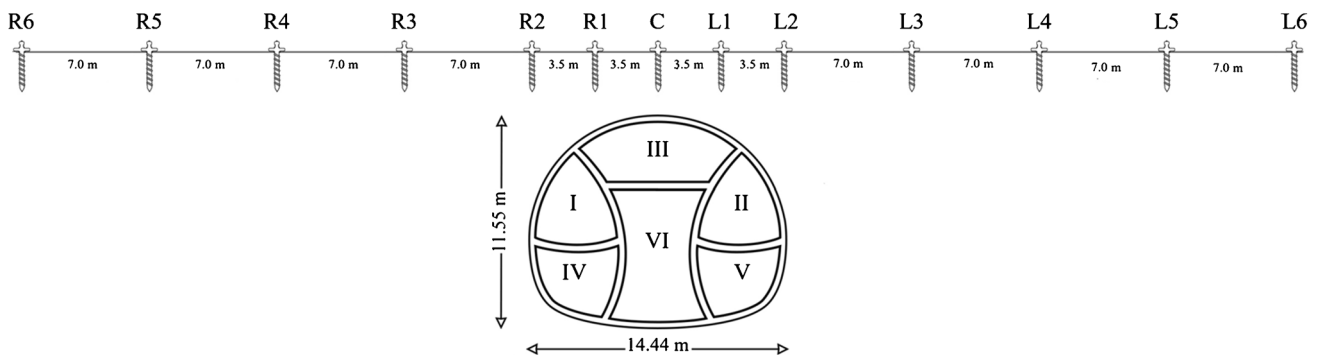


Fig. 12 Typical settlement point layout at a monitoring cross-section

Fig. 13 Vertical displacement of tunnel with time

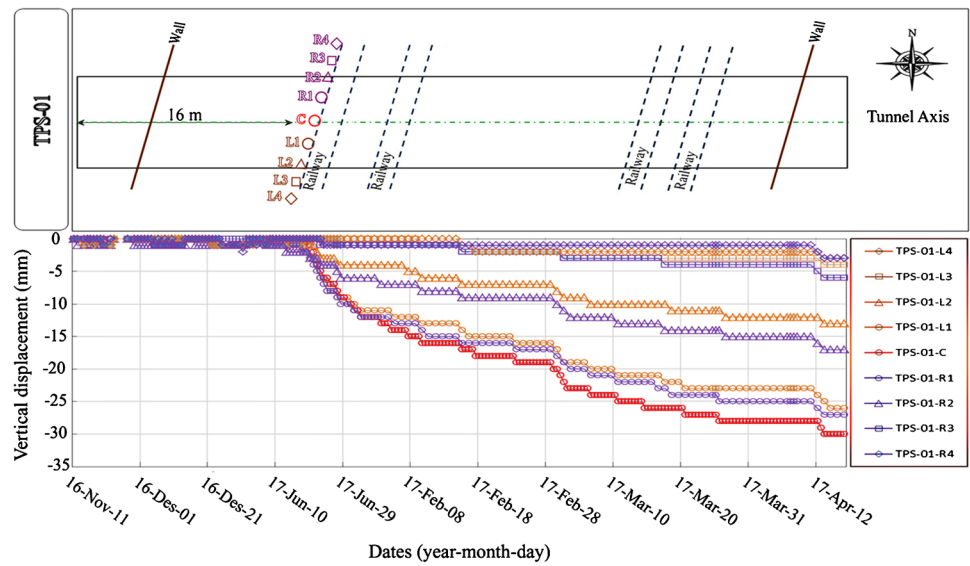
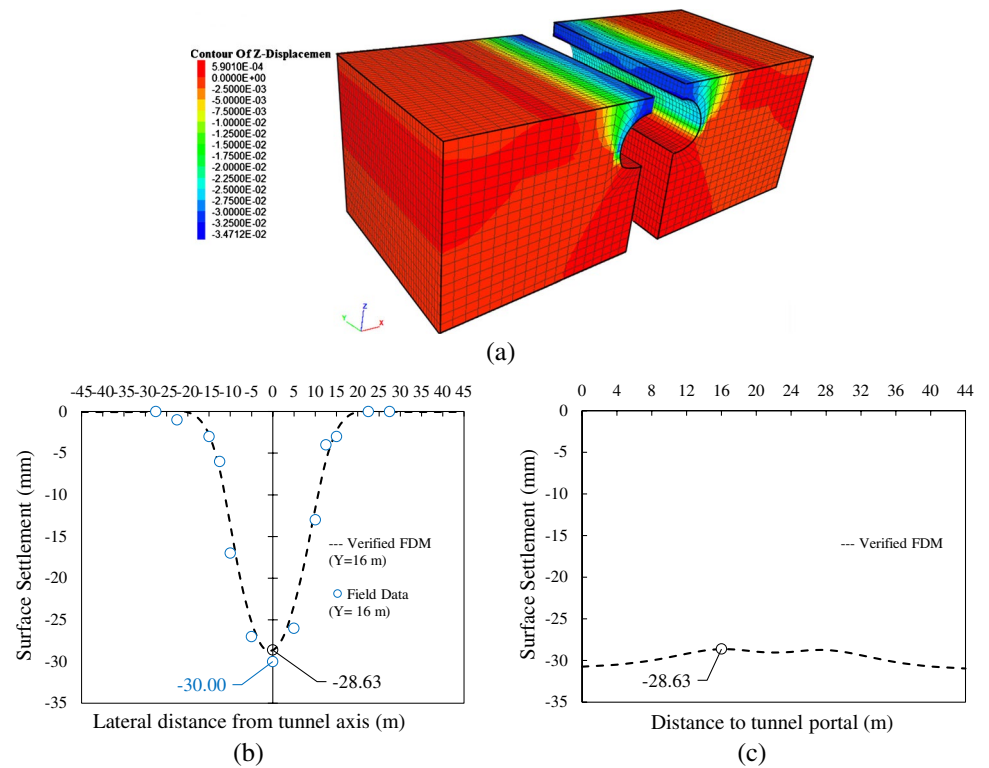


Fig. 14 a Contour of Z_displacement for the verified numerical model (b) comparison of verified FDM results with field measurement data for monitoring section TPS-01 (c) longitudinal settlement profile trough obtained from the verified numerical model



numerical simulation results and the monitored data of surface settlement. Therefore, it could be said that the numerical model is verified.

Random finite difference analysis

In recent years, with the advancement of software technology, RFEM has evolved a lot to study the effect of spatial variability of soil parameters on surface settlement due

to tunneling. In RFEM, the RF of the soil parameters is assigned to the numerical model and then the finite element code is employed to perform the analysis. In this section, the finite element code in the RFEM is replaced by the finite difference program. Therefore, as mentioned earlier, the finite difference software $FLAC^{3D}$ was employed to simulate the excavation of the tunnel. The embedded FISH language in this software is an efficient instrumentation to merge RF into the numerical model.

Implementation of RFDM

By the verified numerical model in the previous section, RF in three-dimensional space can be simulated. For this purpose, the center coordinates of all elements are output and then the one-to-one mapping of RF to the finite difference mesh can be obtained with the language FISH. Thus, a FISH-based program has been evolved in this article. As mentioned in Sect. 2, only the Young's modulus is assumed to be random, but in the Poisson's ratio, unit weight and dilation angle, cohesion and friction angle are given non-random values of $\nu = 0.3$, $\gamma = 1600 \text{ kg/m}^3$, $\psi = 0^\circ$, $C = 29.5 \text{ Kpa}$ and $\varphi = 28^\circ$ respectively. The log-normal distribution is used herein to describe the variability of Young's modulus (Zhu and Zhang 2013) with its mean $E = 27 \text{ MPa}$, and $\text{COV} = 0.2$. As mentioned in Sect. 3.2, to generate RF with exponential function (1) the algorithm presented by Jha and Ching (Jha and Ching 2013) is utilized based on the Fourier series expansion. The FSM creates normally distributed fields. Consequently, for the log-normal field of Young's modulus, the parameters of normal distribution are earned by solving Eq. (4) and (5). Finally, the generated standard RF is transformed using Eq. (6). Some hypotheses are considered to obtain values of SOF. The vertical SOF is assumed 1 m, and both horizontal SOFs (namely θ_x and θ_y) were assumed to be equal (Kawa and Puła 2019).

Seven cases with different horizontal SOFs (i.e., 2, 5, 10, 20, 40, 60 and 100 m) are taken into account. The method used for statistical sampling in the present study is the Monte-Carlo technique. It should be noted that the MCS has the advantages of conceptual simplicity and accuracy in results. However, if MCS and numerical methods are used together, it is usually very time-consuming (Cheng et al. 2019c). The MCS is performed for different values of SOF and for each value of SOF, 1000 random realizations are solved.

Effects of pre-support systems by using the RFDM

As mentioned above, for each intended SOF, 1000 realizations of MCS are carried out. Based upon the accumulated data from each surface settlement curve, both the mean and the COV of S_{\max} are calculated. Figure 15 indicates the variations of the mean and the COV of S_{\max} with SOF in 7 cases. The mean of S_{\max} values obtained by the RFDM is almost equal to the S_{\max} obtained by the verified model. Figure 15b shows that the COV of S_{\max} is increased as the SOF increases and is stabilized for higher values of SOF. Because when SOF is increased beyond $2.8 D$ (D is the width of the tunnel), the strongest correlated areas are expanded both inside and outside of the influence zone. As the induced stress by tunneling is rapidly decreased within an influence zone (Gong et al. 2014), the variations in COV S_{\max} are strongly reduced.

As shown in Fig. 15, the values of both the mean and the COV of S_{\max} remain unchanged as the SOF increases for values greater than 50 m. Therefore, in order to investigate the effects of pre-support systems on S_{\max} , four scenarios with a constant value of the SOF ($\text{SOF} = 60 \text{ m}$) can be considered:

- Installation of both pre-support systems
- Installation of only progressive beam
- Installation of only forepoles
- Lack of pre-support systems installation

It should be noted that to examine the effects of the pre-support systems, for each scenario, 1000 Monte Carlo realizations are performed with a specific SOF ($\text{SOF} = 60 \text{ m}$). Figure 16 shows

an example for scenario D, when realization No.844 is carried out. The value of S_{\max} (about 78.41 mm) and its position in the longitudinal and the transverse settlement profile is obtained from Fig. 16b (see Fig. 16c and 16d). By comparing Fig. 16c and Fig. 14b and also Fig. 16d and Fig. 14c, due to the effects of the spatial variability of the Young's modulus (Fig. 14a), the position of the S_{\max} in the cross-section profile and the longitudinal profile does not

Fig. 15 Variation of (a) Mean of S_{\max} and (b) COV of S_{\max} with different SOFs

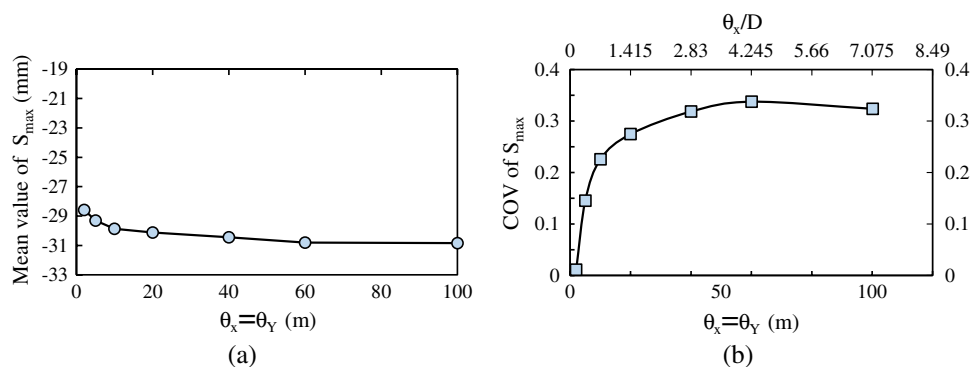
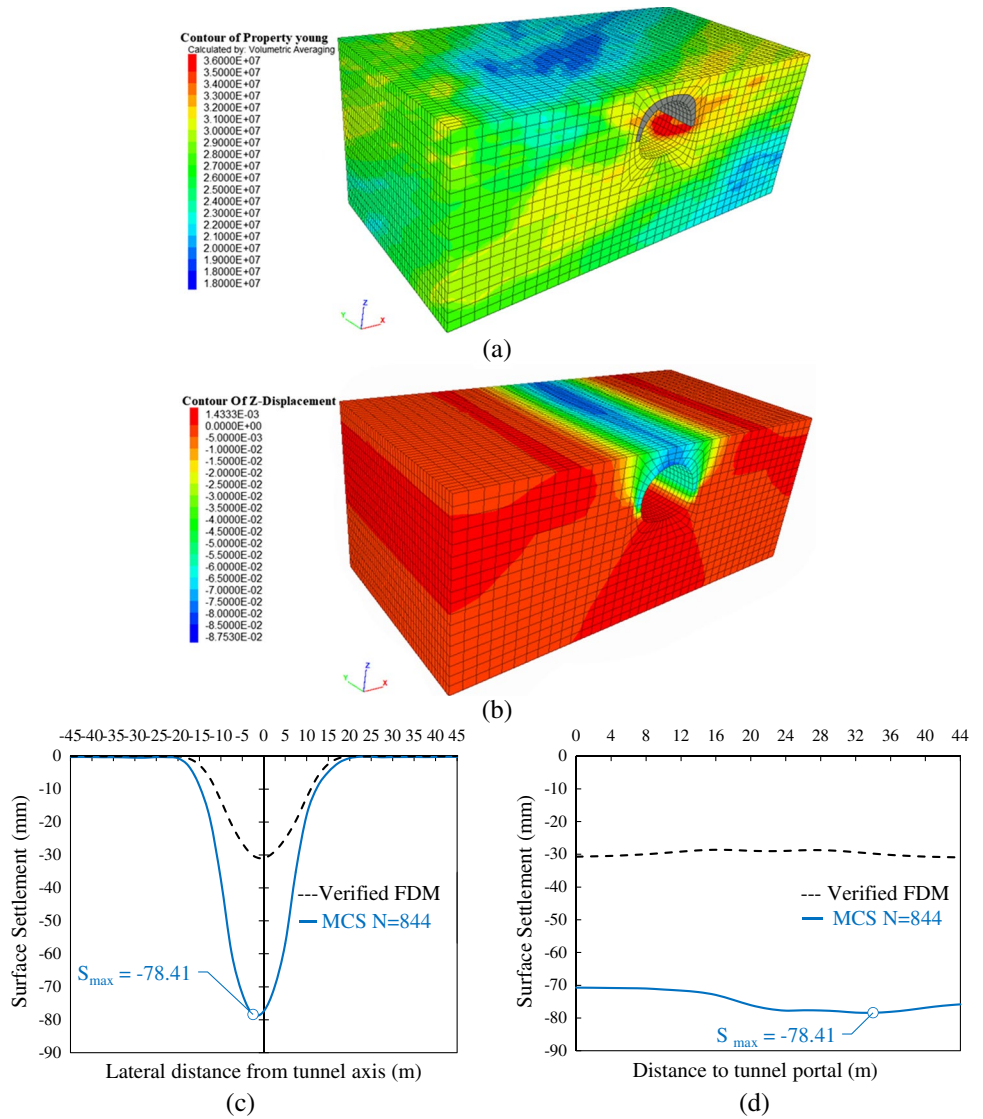


Fig. 16 The obtained results for scenario D, when realization No.844 is carried out; (a) Contour of property of young (b) contour of Z_displacement (C) surface settlement curve in a cross-section that includes S_{max} (d) surface settlement curve in a longitudinal profile that includes S_{max}



appear at the tunnel axis and tunnel entrances (especially eastern portal) respectively.

Therefore, for each scenario, 1000 surface settlement curves are generated and the range of S_{max} in each scenario is obtained. Figures 17 and 18 show the cross-sectional and longitudinal settlement profiles for each scenario. For example, in scenario A, the obtained maximal S_{max} has a range of 5.20 to 80.46 mm (see Figs. 17a and 18a). As shown in Figs. 17 and 18, the position of S_{max} is appeared in different places.

Figure 19 (which is obtained from the data extraction of Figs. 17 and 18) shows the mean and the variation of S_{max} in the case of SOF=60 m based on 1000 runs of the MCS for each scenario. The calculated data from Fig. 19 is listed in Table 5. As shown in this table, scenario A has the lowest mean and COV, contrary to scenario D with the highest mean and COV, compared to other scenarios. Therefore, it can be concluded that both the type of the installed pre-support system and the spatial

variability of the Young’s modulus have a major effect on both the distribution and the magnitude of surface settlement.

One of the important parameters that should be considered during the design and construction of urban tunnels, is the allowable limit of the S_{max} . The choice of the allowable limit (S_{lim}) has an important role in ensuring the stability of the urban tunnels. Therefore, the probability of failure for the S_{max} excessive the S_{lim} should be investigated. The probability of failure can be defined as:

$$P_f = \frac{N_f}{N} \times 100\% \tag{9}$$

where the N =number of realizations (the value of N is set to 1000); N_f =number of the S_{max} exceeding S_{lim} . Figure 20 shows the relationship between the probability of failure and the S_{lim} for various scenarios. It is worth mentioning that for all scenarios, the SOF is set to a constant value (equal 60 m). As expected, the curves in Fig. 18 show that the probability

Fig. 17 Transverse settlement profile and effects of the spatial variability of Young’s modulus on surface displacement: (a) scenario A; (b) scenario B; (c) scenario C; (d) scenario D

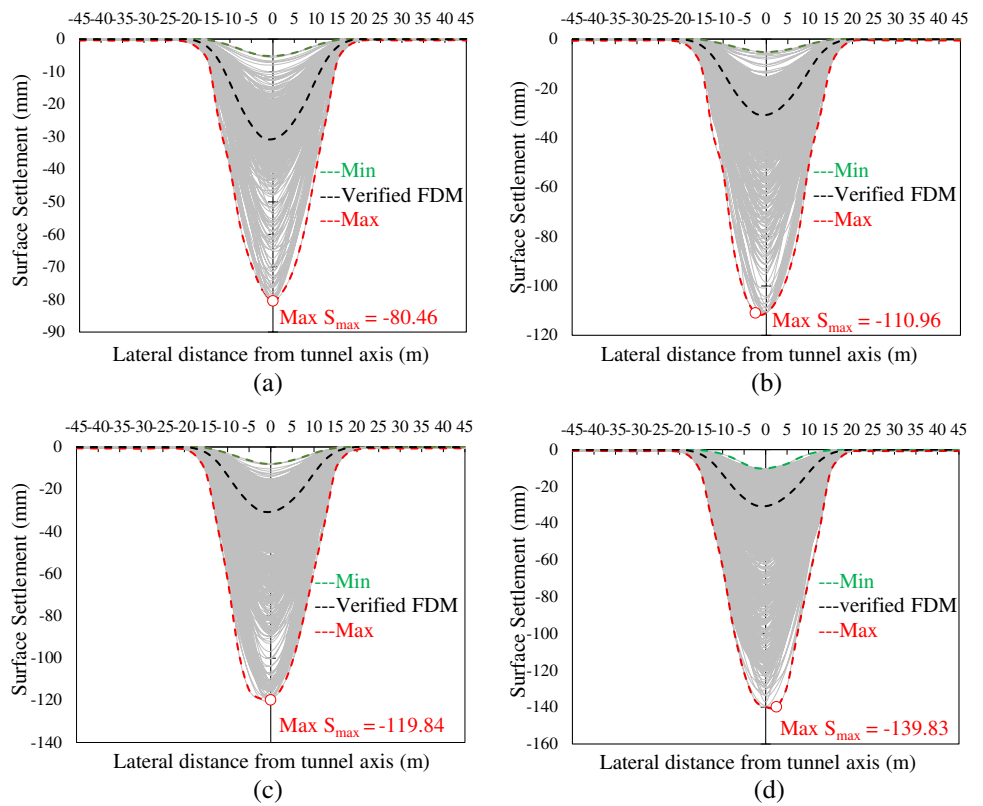


Fig. 18 Longitudinal settlement profile and effects of the spatial variability of Young’s modulus on surface displacement: (a) scenario A; (b) scenario B; (c) scenario C; (d) scenario D

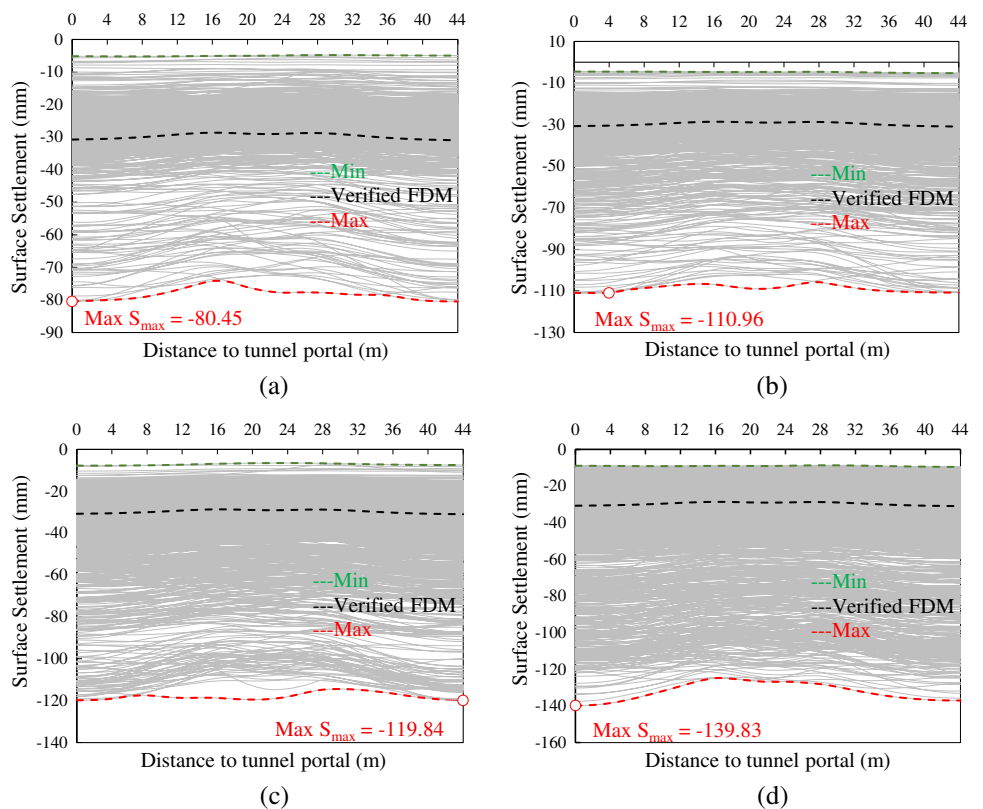


Fig. 19 The values of obtained S_{max} from each scenarios: (a) scenario A; (b) scenario B; (c) scenario C; (d) scenario D

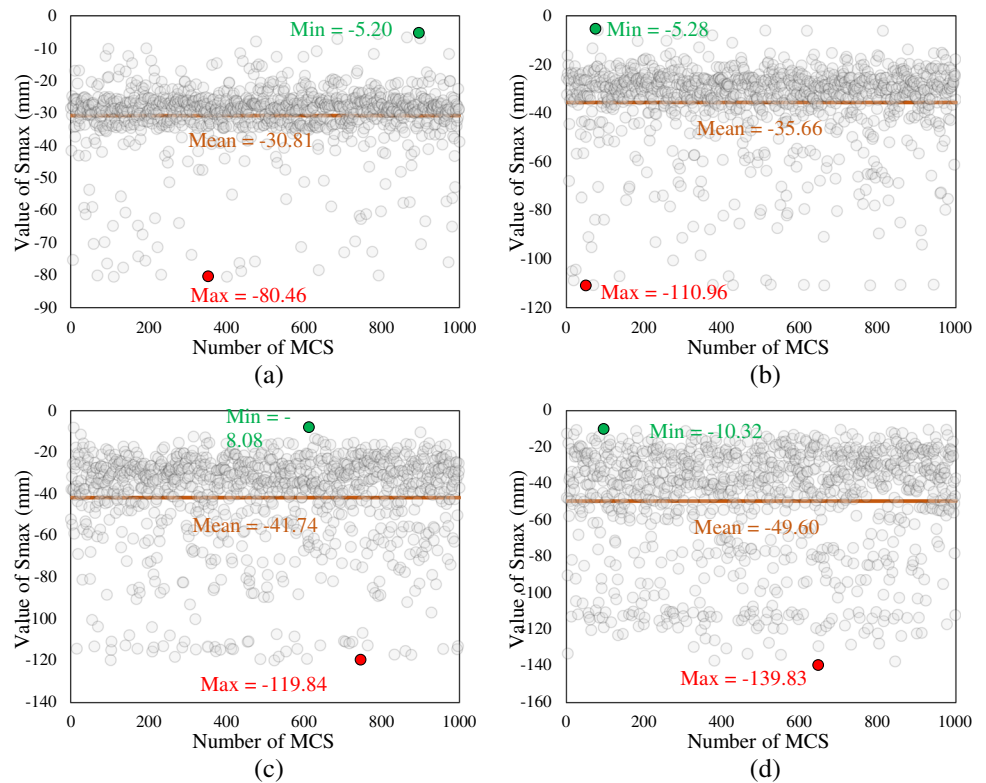


Table 5 Results of obtained from 1000 Monte Carlo realizations, when SOF= 60 m

Scenario	Mean of S_{max} (mm)	COV of S_{max}	Min of S_{max} (mm)	Max of S_{max} (mm)
A	-30.808	0.338	-5.201	-80.458
B	-35.665	0.487	-5.275	-110.956
C	-41.740	0.558	-8.077	-119.840
D	-49.601	0.622	-10.325	-139.832

of failure increases for the allowable limit smaller than the S_{max} of verified FDM and decreases for the allowable limit greater than the S_{max} of verified FDM. As an example, when a level of $S_{lim} = 35$ mm is selected, the probability of failure for scenarios A and D is 13% and 59.1%, respectively.

Figure 20 clearly shows that scenario A and D have the lowest and highest probability of failure respectively among all scenarios for all values of S_{lim} .

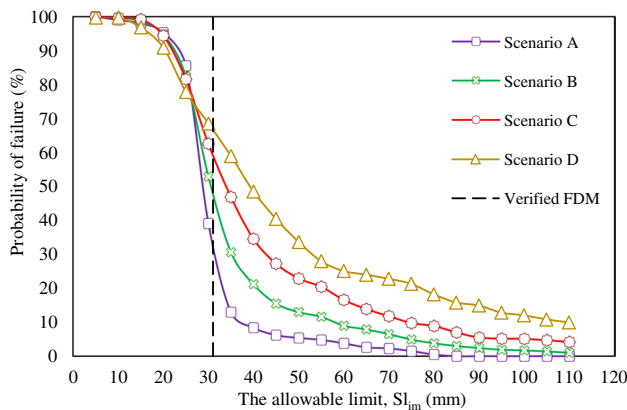


Fig. 20 Probability of failure of the maximal surface settlement exceeding the allowable limit S_{lim} for various scenarios

Conclusions

- 1- Despite the installation of support systems, with the consideration of the spatial variability of the soil, the S_{max} increases from 30 to 80 mm. So, the soil should not be considered homogeneous in the probabilistic analysis and the engineering design.
- 2- By comparing A and D scenarios, the COV of S_{max} and mean of S_{max} increase significantly from 0.33 to 0.62 (about 84%) and 31 mm to 50 mm (about 61%), respectively, which shows its influence on the distribution of the weak strength regions in the influence scope of the tunnel when SOF has constant value.
- 3- When SOF is considered 60 m, the Young’s modulus is strongly correlated spatially in a larger range and the geological properties in the numerical model can be more similar to the geological conditions of the project studied

case; therefore, the maximum number of the variations of S_{\max} occurs in the range of 0 to 45 mm (see Fig. 19)

- 4- By comparing B and C scenarios, the progressive beam among pre-support systems plays the largest role in reducing the surface settlement.

Funding No funds, grants, or other support was received for preparing this article.

Declarations

Conflicts of interest The authors have no conflicts of interest to declare that are relevant to the content of this article.

References

- Bagińska I, Kawa M, Janecki W (2016) Estimation of spatial variability of lignite mine dumping ground soil properties using CPTu results. *Studia Geotechnica et Mechanica* 38:3–13. <https://doi.org/10.1515/sgem-2016-0001>
- Carranza-Torres C, Diederichs M (2009) Mechanical analysis of circular liners with particular reference to composite supports. For example, liners consisting of shotcrete and steel sets. *Tunn Undergr Space Technol* 24:506–532. <https://doi.org/10.1016/j.tust.2009.02.001>
- Cheng H, Chen J, Chen R, Chen G (2019a) Comparison of Modeling Soil Parameters Using Random Variables and Random Fields in Reliability Analysis of Tunnel Face. *Int J Geomech* 19:04018184. [https://doi.org/10.1061/\(ASCE\)GM.1943-5622.0001330](https://doi.org/10.1061/(ASCE)GM.1943-5622.0001330)
- Cheng H, Chen J, Chen R, Huang J, Li J (2019b) Three-dimensional analysis of tunnel face stability in spatially variable soils. *Comput Geotech* 111:76–88. <https://doi.org/10.1016/j.compgeo.2019.03.005>
- Cheng H, Chen J, Li J (2019c) Probabilistic Analysis of Ground Movements Caused by Tunneling in a Spatially Variable Soil. *Int J Geomech* 19:04019125. [https://doi.org/10.1061/\(ASCE\)GM.1943-5622.0001526](https://doi.org/10.1061/(ASCE)GM.1943-5622.0001526)
- Cherubini C (1997) Data and considerations on the variability of geotechnical properties of soils. In: *Proceedings of the Conference on Advances in Safety and Reliability, ESREL*. pp 1583–1591
- Dasaka S, Zhang L (2012) Spatial variability of in situ weathered soil. *Géotechnique* 62:375–384. <https://doi.org/10.1680/geot.8.P.151.3786>
- Dehghani NL, Rahimi M, Shafieezadeh A, Padgett JE (2020) Parameter Estimation of a Fractional Order Soil Constitutive Model Using KiK-Net Downhole Array Data: A Bayesian Updating Approach. *Geo-Congress 2020*:346–356. <https://doi.org/10.1061/9780784482810.037>
- Fenton GA, Griffiths DV (2008) *Risk assessment in geotechnical engineering* vol 461. John Wiley & Sons New York,
- Fenton GA, Griffiths D (2002) Probabilistic foundation settlement on spatially random soil. *J Geotech Geoenvironmental Eng* 128:381–390
- Fenton GA, Griffiths D (2003) Bearing-capacity prediction of spatially random c ϕ soils. *Can Geotech J* 40:54–65. <https://doi.org/10.1139/t02-086>
- Fenton GA, Griffiths D (2005) Three-dimensional probabilistic foundation settlement. *J Geotech Geoenvironmental Eng* 131:232–239
- Gong W, Luo Z, Juang CH, Huang H, Zhang J, Wang L (2014) Optimization of site exploration program for improved prediction of tunneling-induced ground settlement in clays. *Comput Geotech* 56:69–79. <https://doi.org/10.1016/j.compgeo.2013.10.008>
- Griffiths DV, Fenton G (2008) *Risk assessment in geotechnical engineering* John Wiley & Sons, Inc:381–400
- Griffiths D, Fenton GA (2001) Bearing capacity of spatially random soil: the undrained clay Prandtl problem revisited. *Geotechnique* 51:351–359. <https://doi.org/10.1680/geot.51.4.351.39396>
- Griffiths D, Fenton G (2004) Probabilistic slope stability analysis by finite elements. *J Geotech Geoenviron* 130(5):507–518
- He B-G, Zhang X-W, Li H-P (2019) Ground load on tunnels built using new Austrian tunneling method: study of a tunnel passing through highly weathered sandstone. *Bull Eng Geol Env* 78:6221–6234
- Huang J, Lyamin A, Griffiths D, Krabbenhoft K, Sloan S (2013) Quantitative risk assessment of landslide by limit analysis and random fields. *Comput Geotech* 53:60–67. <https://doi.org/10.1016/j.compgeo.2013.04.009>
- Jaksa MB, Brooker PI, Kaggwa WS (1997) Inaccuracies Associated with Estimating Random Measurement Errors. *J Geotech Geoenvironmental Eng* 123:393–401. [https://doi.org/10.1061/\(ASCE\)1090-0241\(1997\)123:5\(393\)](https://doi.org/10.1061/(ASCE)1090-0241(1997)123:5(393))
- Jaky J (1948) Pressure in silos Proc 2nd ICSM, 1948
- Jha SK, Ching J (2013) Simplified reliability method for spatially variable undrained engineered slopes. *Soils Found* 53:708–719. <https://doi.org/10.1016/j.sandf.2013.08.008>
- Karamiayi FM, Dehghan A (2019) The Effect of Pre-Support System (Fore-poling) on the Control of Ground Surface Subsidence caused by SEM/NATM in Shallow Urban Road Tunnels under Railway Traffic Loading
- Kawa M, Puła W (2019) 3D bearing capacity probabilistic analyses of footings on spatially variable c - ϕ soil. *Acta Geotechnica*. <https://doi.org/10.1007/s11440-019-00853-3>
- Li D-Q, Jiang S-H, Cao Z-J, Zhou W, Zhou C-B, Zhang L-M (2015) A multiple response-surface method for slope reliability analysis considering spatial variability of soil properties. *Eng Geol* 187:60–72. <https://doi.org/10.1016/j.enggeo.2014.12.003>
- Lumb P (1966) The variability of natural soils. *Can Geotech J* 3:74–97. <https://doi.org/10.1139/t66-009>
- Marinos V, Goricki A, Malandrakis E (2019) Determining the principles of tunnel support based on the engineering geological behaviour types: example of a tunnel in tectonically disturbed heterogeneous rock in Serbia. *Bull Eng Geol Env* 78:2887–2902. <https://doi.org/10.1007/s10064-018-1277-7>
- Miro S, König M, Hartmann D, Schanz T (2015) A probabilistic analysis of subsoil parameters uncertainty impacts on tunnel-induced ground movements with a back-analysis study. *Comput Geotech* 68:38–53. <https://doi.org/10.1016/j.compgeo.2015.03.012>
- Möller SC (2006) Tunnel induced settlements and structural forces in linings. Univ. Stuttgart, Inst. f. Geotechnik Stuttgart, Germany
- Mollon G, Dias D, Soubra A-H (2013) Probabilistic analyses of tunneling-induced ground movements. *Acta Geotech* 8:181–199. <https://doi.org/10.1007/s11440-012-0182-7>
- Moosavi E, Shirinabadi R, Rahimi E, Gholinejad M (2018) Numerical Modeling of Ground Movement due to Twin Tunnel Structure of Esfahan Subway, Iran. *J Min Sci* 53:663–675. <https://doi.org/10.1134/S1062739117042655>
- Phoon K-K, Kulhawy FH (1999) Characterization of geotechnical variability. *Can Geotech J* 36:612–624. <https://doi.org/10.1139/t99-038>
- Rahimi M, Wang Z, Shafieezadeh A, Wood D, Kubatko EJ (2020) Exploring Passive and Active Metamodeling-Based Reliability Analysis Methods for Soil Slopes: A New Approach to Active Training. *Int J Geomech* 20:04020009
- Taromi M, Eftekhari A, Hamidi JK, Aalianvari A (2017) A discrepancy between observed and predicted NATM tunnel behaviors and updating: a case study of the Sabzkuh tunnel. *Bull Eng Geol Env* 76:713–729. <https://doi.org/10.1007/s10064-016-0862-x>
- Vanmarcke E (1983) *Random fields: analysis and synthesis*. The MIT Press, Cambridge, Mass
- Vanmarcke E (2010) *Random fields: analysis and synthesis*. World Scientific
- Xiao L, Huang H, Zhang J (2017) Effect of soil spatial variability on ground settlement induced by shield tunnelling. In: *Geo-Risk 2017*. pp 330–339
- Zhou X-P, Zhu B-Z, Juang C-H, Wong LNY (2019) A stability analysis of a layered-soil slope based on random field. *Bull Eng Geol Env* 78:2611–2625. <https://doi.org/10.1007/s10064-018-1266-x>
- Zhu H, Zhang LM (2013) Characterizing geotechnical anisotropic spatial variations using random field theory. *Can Geotech J* 50:723–734